



Engineered neuronal microtissue provides exogenous axons for delayed nerve fusion and rapid neuromuscular recovery in rats

Justin C. Burrell^{a,b,c}, Suradip Das^{a,c}, Franco A. Laimo^{a,c}, Kritika S. Katiyar^{a,d}, Kevin D. Browne^{a,c}, Robert B. Shultz^{a,d}, Vishal J. Tien^{a,b,c}, Phuong T. Vu^{a,b,c}, Dmitriy Petrov^a, Zarina S. Ali^a, Joseph M. Rosen^e, D. Kacy Cullen^{a,b,c,d,*}

^a Center for Brain Injury & Repair, Department of Neurosurgery, Perelman School of Medicine, University of Pennsylvania, Philadelphia, PA, USA

^b Department of Bioengineering, School of Engineering & Applied Science, University of Pennsylvania, Philadelphia, PA, USA

^c Center for Neurotrauma, Neurodegeneration & Restoration, Corporal Michael J. Crescenz Veterans Affairs Medical Center, Philadelphia, PA, 19104, USA

^d Axonova Medical, LLC, Philadelphia, PA, USA

^e Dartmouth-Hitchcock Medical Center, Division of Plastic Surgery, Dartmouth College, Lebanon, NH, USA

ARTICLE INFO

Keywords:

Nerve regeneration
Neuromuscular injury
Muscle preservation
Tissue engineering
Microtissue
Axon fusion

ABSTRACT

Nerve injury requiring surgical repair often results in poor functional recovery due to the inability of host axons to re-grow long distances and reform meaningful connections with the target muscle. While surgeons can re-route local axon fascicles to the target muscle, there are no technologies to provide an exogenous source of axons without sacrificing healthy nerves. Accordingly, we have developed tissue engineered neuromuscular interfaces (TE-NMIs) as the first injectable microtissue containing motor and sensory neurons in an anatomically-inspired architecture. TE-NMIs provide axon tracts that are intended to integrate with denervated distal structures and preserve regenerative capacity during prolonged periods without host innervation. Following implant, we found that TE-NMI axons promoted Schwann cell maintenance, integrated with distal muscle, and preserved an evoked muscle response out to 20-weeks post nerve transection in absence of innervation from host axons. By repopulating the distal sheath with exogenous axons, TE-NMIs also enabled putative delayed fusion with proximal host axons, a phenomenon previously not achievable in delayed repair scenarios due to distal axon degeneration. Here, we found immediate electrophysiological recovery after fusion with proximal host axons and improved axon maturation and muscle reinnervation at 24-weeks post-transection (4-weeks following delayed nerve fusion). These findings show that TE-NMIs provide the potential to improve functional recovery following delayed nerve repair.

1. Introduction

Peripheral nerve injury (PNI) has been estimated to present in 3% of trauma case and up to 5% if including plexus and root avulsion injuries [1–3]. More than 550,000 PNI procedures are performed annually in the U.S [4]. Despite recent advancements in peripheral nerve repair, it is estimated that only 50% of patients will achieve satisfactory functional recovery [5]. Although several factors impact successful regeneration, delayed surgical repair is considered one of the most important contributing factors to poor functional recovery [6,7]. After injury, axons in the distal nerve undergo Wallerian degeneration. Dedifferentiated Schwann cells temporarily form columnar pro-regenerative

structures called the bands of Büngner that promote axon regeneration and targeted muscle reinnervation [8]. Over time, prolonged denervation due to the loss of axonal contact leads to the degradation of the bands of Büngner, diminishing the potential for muscle reinnervation and ultimately functional recovery [9]. Unfortunately, delayed repairs are common in cases of polytrauma resulting in severe nerve trauma because surgeons will prioritize lifesaving procedures. Moreover, clinicians often utilize a “wait-and-see” approach in cases where it is unclear whether repair is necessary (i.e. stretch nerve injury) to ascertain potential spontaneous recovery. Nerve transfers are an innovative surgical approach that have become increasingly common for restoring functionality after severe nerve injury by providing early reinnervation of

Peer review under responsibility of KeAi Communications Co., Ltd.

* Corresponding author. 105E Hayden Hall/3320 Smith Walk, Dept. of Neurosurgery, University of Pennsylvania, Philadelphia, PA, 19104.

E-mail address: dkacy@pennmedicine.med.upenn.edu (D.K. Cullen).

<https://doi.org/10.1016/j.bioactmat.2022.03.018>

Received 6 December 2021; Received in revised form 18 February 2022; Accepted 11 March 2022

Available online 24 March 2022

2452-199X/© 2022 The Authors. Publishing services by Elsevier B.V. on behalf of KeAi Communications Co. Ltd. This is an open access article under the CC BY-NC-ND license (<http://creativecommons.org/licenses/by-nc-nd/4.0/>).

denervated muscle using ectopic/donor axons from a healthy nearby nerve and/or fascicle(s). However, nerve transfers are only indicated in specific surgical scenarios and require the sacrifice of an otherwise uninjured nerve or fascicle(s). Thus, there is a clinical unmet need for a novel strategy that can prolong the effective surgical window to improve the likelihood for meaningful recovery.

Recently, the direct connection of two cut axons ends – termed “fusion” and facilitated by fusogens, such as polyethylene glycol (PEG) – has gained significant interest due to potential for immediately restoring electrical conduction following repair [10]. Although the exact mechanism is unclear, fusion has been reported to improve functional recovery likely by hastening reinnervation [10–20]. However, successful fusion requires fusible axons in the distal stump, therefore, the clinical indication for fusion may be limited to less than 3 days post-injury or the period before Wallerian degeneration and distal axon fragmentation [21]. Thus, although nerve fusion is a promising strategy, additional preclinical and clinical testing is necessary to determine whether this approach would be indicated for the widespread patient population requiring delayed nerve repair.

To address the clinical challenges limiting functional recovery following delayed nerve repair, our group has developed tissue engineered neuromuscular interfaces (TE-NMIs) as a minimally-invasive “babysitting” strategy to deliver a bolus of exogenous neurons – and importantly their axon projections – for preservation of the pro-regenerative Schwann cells and early muscle reinnervation. By advancing microtissue engineering strategies pioneered by our group [22–26], TE-NMIs are comprised of populations of spinal motor neurons and/or sensory neurons spanned by long axonal tracts within a protective hydrogel outer encasement. In this study, TE-NMI characterization of motor and sensory neurite growth was compared in various biomaterial outer encasements. Next, the potential for TE-NMIs to serve as a suitable Schwann cell and muscle “babysitting” strategy was investigated by assessing TE-NMI survival and axonal outgrowth, Schwann cell preservation, and muscle innervation in a rodent model of prolonged axotomy. Finally, the ability for TE-NMIs to enable delayed axon fusion and facilitate neuromuscular recovery following direct nerve coaptation was evaluated. Based on the findings in this study, TE-NMIs may represent a transformative strategy for simultaneously mitigating the

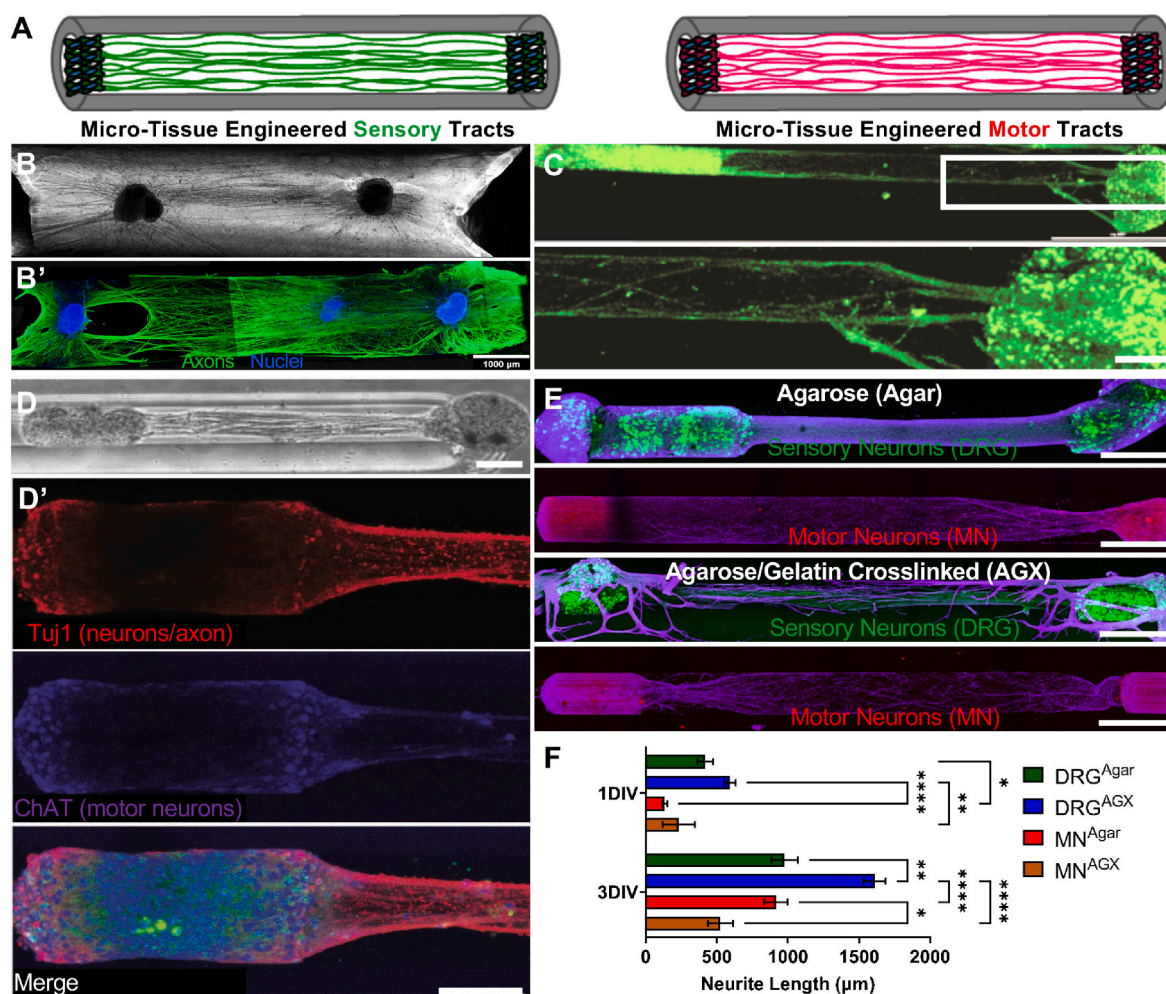


Fig. 1. Tissue Engineered Neuromuscular Interfaces (TE-NMIs) Fabrication and Characterization. (A) TE-NMIs are anatomically-inspired bioengineered microtissue with discrete neuron populations spanned by sensory, motor, or both motor and sensory axon tracts within a protective biomaterial encasement. The modular TE-NMI fabrication process allows for construction of micro-column hydrogels with various diameters, neuronal cell sources, or biomaterial outer encasement. (B) Representative phase and (B') confocal images are shown of a sensory TE-NMI with a 2 mm outer diameter and 1 mm inner diameter labeled with Tuj1, a neuronal/axonal marker (green) and counterstained with hoechst (blue) to identify nuclei. (C) Representative confocal image of a motor TE-NMI with a 350 μm outer and 180 μm inner diameter at 7 days *in vitro* (DIV) that was virally transduced to express green fluorescent protein (GFP). (D) At 14 DIV, phase imaging revealed two discrete populations of motor neurons (MNs) spanned by axons. (D') High resolution confocal imaging revealed discrete regions of motor neurons/axons labeled for Tuj1, ChAT, a motor neuron specific marker, and hoechst. (E) Representative confocal images at 7 DIV of constructs with an agarose or an agarose-gelatin composite (AGX) outer encasement. (G) Neurite length within each biomaterial encasement was compared at 1 and 3 DIV. Mean values compared using two-way ANOVA. Error bars represent standard error. *p < 0.05; **p < 0.01; ****p < 0.0001. Scale bars: (C–D) 500 μm, zoom in: 100 μm. (E–H) 500 μm.

deleterious effects of prolonged denervation and enabling delayed axon fusion, thus potentially providing improved functional recovery even in cases of delayed nerve repair.

2. Results

2.1. Tissue engineered neuromuscular interfaces (TE-NMIs) are performed axon-rich microtissue within a protective biomaterial

TE-NMIs are anatomically-inspired neural constructs comprised of discrete populations of neurons spanned by long axon tracts similar to the neuronal-axonal organization of the nervous system (Fig. 1). Building on previous work [27], we have engineered microtissue comprised of sensory neurons-axons alone (sensory TE-NMI), motor neurons-axons alone (motor TE-NMI) or a mixed population of motor and sensory neurons-axons (mixed TE-NMI) (Fig. 1A). In an initial experiment, robust sensory axon growth was observed spanning dorsal root ganglia (DRG) spaced 5 mm apart in large macro-scale agarose columns with a 2 mm outer diameter and 1 mm inner diameter containing collagen extracellular matrix (ECM) (Fig. 1B). Next, microtissue engineering fabrication techniques were adapted from methodology previously developed in our lab for Parkinson's disease, spinal cord injury, and brain-machine interfacing [28–30]. The smallest TE-NMI was 3 mm long with a 350 μm outer and 180 μm inner diameter (Fig. 1C); however, since our goal was to match the fascicular structure in the nerve, unless otherwise noted, TE-NMI in the following studies were 3–5 mm long with a 701 μm outer and 300 μm inner diameter.

For motor and mixed TE-NMIs, aggregated embryonic spinal motor neuron populations were formed as described previously [31], and then plated on the end of the micro-column. Healthy neurons and neurite outgrowth were observed via phase-microscopy. TE-NMI immunocytochemistry confirmed the motor neuron phenotype with the co-labeling of Tuj1, a neuronal/axonal marker, and ChAT (Fig. 1D). Agarose is a relatively inert biomaterial but it has a long degradation time into non-resorbable byproducts that may hinder translation. Therefore, alternative bioencasement consisting of an agarose-gelatin composite hydrogel were assessed (Fig. 1E). At 1 day *in vitro* (DIV), sensory outgrowth in an agarose-gelatin micro-column was faster than motor outgrowth in either an agarose or agarose-gelatin micro-column. However, by 3 DIV, although sensory outgrowth in an agarose-gelatin micro-column was greater than the other groups, increased motor outgrowth was found in the agarose micro-column compared to the agarose-gelatin micro-column (Fig. 1F). These findings corroborate previous work showing sensory axons extending from DRG explants is often faster than motor neurons aggregates [32]. Interestingly, these data suggest motor neurons preferentially grow in agarose micro-columns despite the presence of active moieties in the agarose-gelatin microcolumns. To evaluate preferential outgrowth from motor or sensory neurons, neurite outgrowth was measured within a mixed TE-NMI. Presence of sensory neurons on one end of the TE-NMI significantly enhanced motor outgrowth by 3 DIV (Fig. S1). Based on these findings, agarose micro-columns were selected for *in vivo* experiments to improve the likelihood for successful motor outgrowth while providing protection from the host immune response following transplantation.

2.2. TE-NMIs preserve Schwann cells in an otherwise denervated nerve at 6 weeks post transplantation

To evaluate whether TE-NMIs can preserve the regenerative capacity of the distal nerve, the sciatic nerve was cut, TE-NMIs were attached to the distal nerve, and the proximal stump was capped to prevent host regeneration (Fig. 2A) [33]. At two weeks, robust transplanted TE-NMI neurons and axons were found within the lumen protected by the outer encasement following optical clearing and two-photon microscopy (Fig. 2B). In this study, one or two TE-NMIs (1x or 2x, respectively) were

transplanted in a conduit secured to the distal stump of the sciatic nerve. We hypothesized that early reinnervation of the otherwise denervated Schwann cells with TE-NMI axons would preserve Schwann cell expression following prolonged host axotomy. Notably, host S100 β + Schwann cells closely aligned with GFP + axons and in some cases, GFP + axons were visualized extending through Schwann cells resembling bands of Büngner (Fig. 2C). Indeed, at 6 weeks post transplantation, robust sensory TE-NMI axon outgrowth was found extending at least 5 mm within the host tissue (Fig. 2D). Following implantation of 2x TE-NMIs, greater GFP + axonal outgrowth was found compared to controls ($F(2,9) = 11.49$; $p < 0.005$; Fig. 2E).

S100 β + Schwann cells and C-Jun expression, in context with total cell counts based on nuclear (Hoechst+) staining, were also quantified at 6 weeks following transplantation using automatic segmentation (Fig. 2F). The total number of Hoechst + cells was greater in the 2x TE-NMI cohort (303.3 ± 49.35 cells/ $40,000 \mu\text{m}^2$) than the acellular group (202.2 ± 41.36 cells/ $40,000 \mu\text{m}^2$; $F(2, 9) = 4.44$; $p = 0.0376$; Fig. 2G). Additionally, of the Hoechst + cells, greater co-expression of S100 β was found in the 2x TE-NMI group (249.1 ± 30.29 cells/ $40,000 \mu\text{m}^2$) than the 1x TE-NMI (155.2 ± 17.91 cells/ $40,000 \mu\text{m}^2$; $p = 0.0038$) or acellular cohorts (141.2 ± 10.22 cells; $F(2, 9) = 15.78$; $p = 0.0015$; Fig. 2I). Similarly, of the Hoechst- and S100 β + cells, greater co-localization with C-Jun was observed in the 2x TE-NMI cohort (249.1 ± 15.14 cells/ $40,000 \mu\text{m}^2$) than the 1x TE-NMI (155.2 ± 35.82 cells/ $40,000 \mu\text{m}^2$; $p = 0.0095$) or acellular groups (141.2 ± 20.44 cells/ $40,000 \mu\text{m}^2$; $F(2, 9) = 9.883$; $p = 0.0102$; Fig. 2J). Interestingly, we also found increased C-Jun expression in the 2x TE-NMI cohort (517.5 ± 71.06 cells/ $40,000 \mu\text{m}^2$) compared to the 1x TE-NMI (225.1 ± 23.09 cells/ $40,000 \mu\text{m}^2$; $p = 0.0003$) and acellular groups (239.1 ± 83.77 cells/ $40,000 \mu\text{m}^2$; $F(2, 9) = 25.91$; $p = 0.0005$; Fig. 2H). These findings suggest that exogenous axons extending from TE-NMIs may maintain the pro-regenerative environment necessary for regenerating host axons to reinnervate distal end targets following repair.

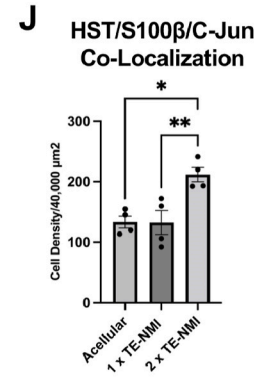
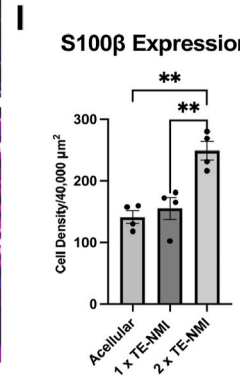
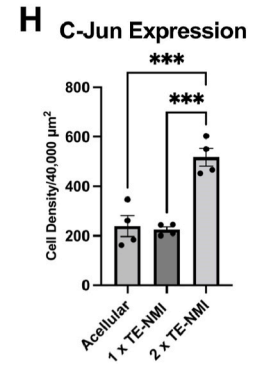
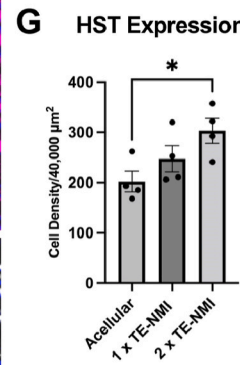
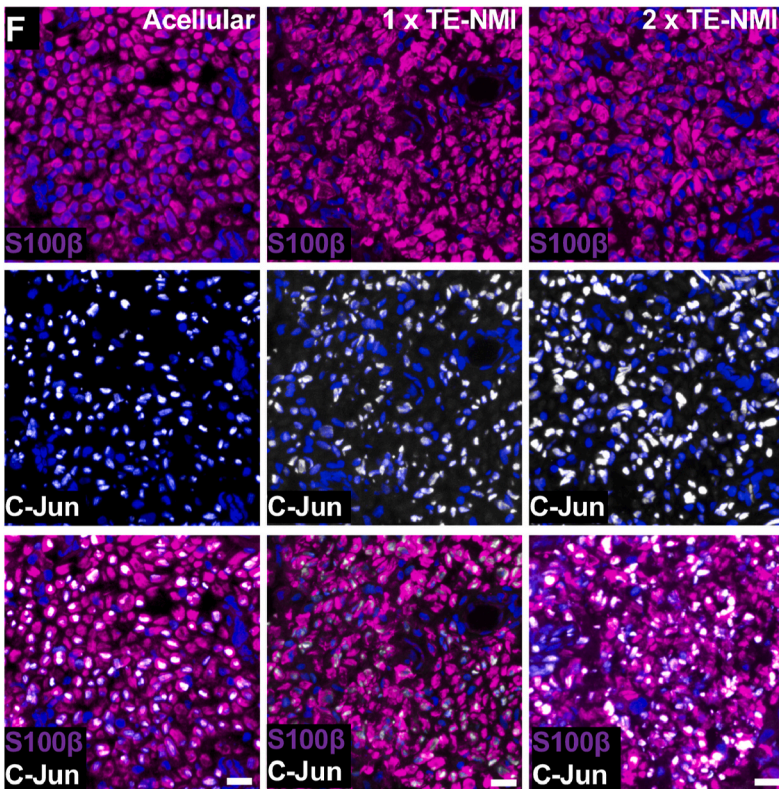
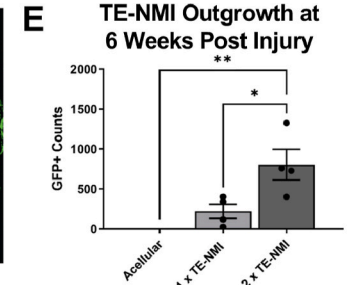
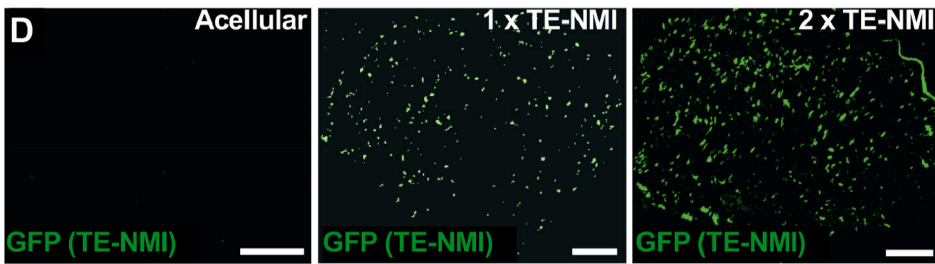
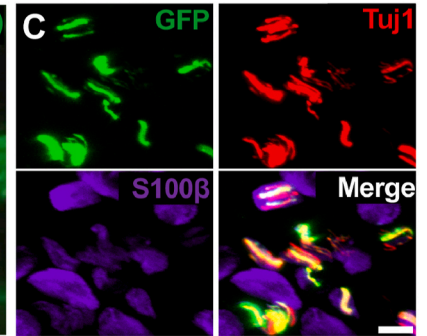
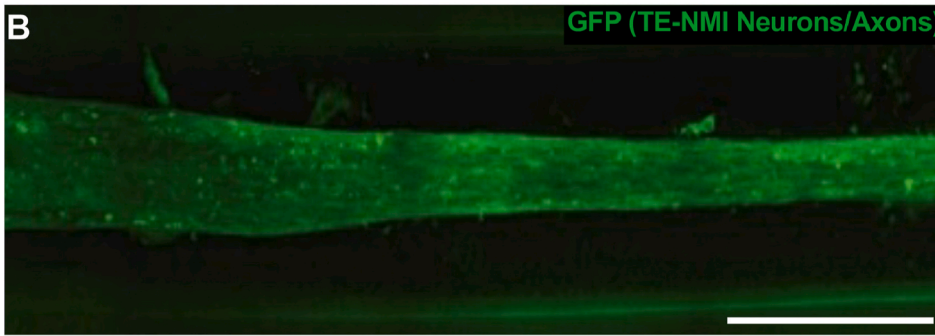
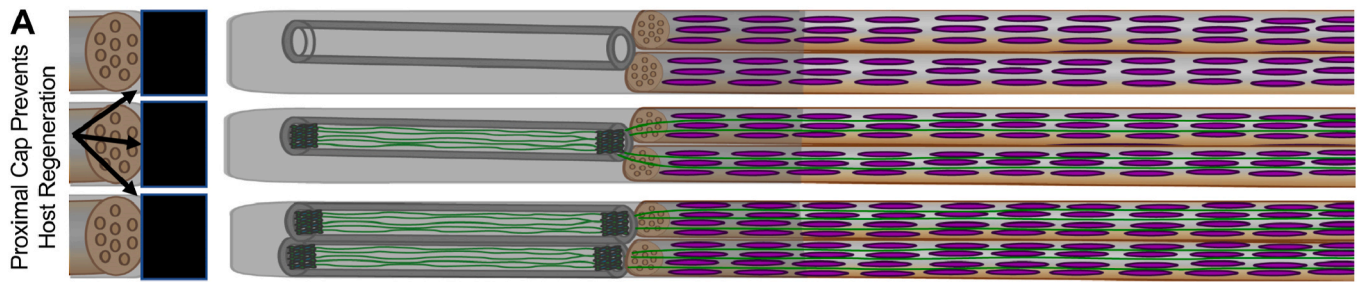
2.3. TE-NMIs maintain distal muscle target electrophysiological activity at 16 weeks post transplantation

Next, we investigated whether mixed sensory-motor TE-NMIs can preserve the otherwise denervated muscle (Fig. 3). Mixed motor-sensory TE-NMIs (Fig. 3A) were chosen as sensory axons were efficacious in preserving Schwann cells and we postulated that the addition of motor axons will be beneficial to preserve the muscle electrophysiological response following chronic host axotomy [33]. The distal common peroneal nerve was selected for the surgical paradigm as the mono-fascicular nerve architecture more closely matched the TE-NMI diameter, avoiding the need for multiple constructs. After securing the TE-NMI to the otherwise denervated distal common peroneal nerve, the transected proximal nerve stump was attached to the neighboring muscle to prevent host regeneration (Fig. 3B).

To test whether mixed TE-NMIs integrated with the otherwise denervated distal muscle target, percutaneous stimulation was performed at 16 weeks post transplantation. A robust evoked muscle response was observed in all animals in the mixed TE-NMI group despite the lack of host axons due to the proximal nerve cap preventing host regeneration (Fig. 3C, D). The mean amplitude of the evoked muscle response for the TE-NMI group was 2.3 ± 0.96 mV, which was approximately 5–6 times greater than response in the control groups (acellular micro-column: 0.4 ± 0.43 mV; no implant: 0.4 ± 0.61 mV; $F(2,12) = 12.18$; $p = 0.0013$). These findings indicate that exogenous TE-NMI axons integrate with the otherwise denervated muscle and likely preserve its ability to generate an evoked muscle response.

2.4. TE-NMIs provide exogenous axons in the otherwise denervated distal nerve sheath to enable delayed axon fusion

Based on these findings, we hypothesized that TE-NMI axons



(caption on next page)

Fig. 2. TE-NMI Survival, Outgrowth, and Integration with the Otherwise Denervated Nerve. (A) Schematic illustrating the chronic host axotomy surgical model and experimental groups, including transplantation of an acellular column, one TE-NMI, or two TE-NMI. Acellular controls were transplanted as negative controls. We hypothesized that TE-NMI would extend axons that interact with the Schwann cells in the otherwise denervated distal nerve. (B) Representative image of a micro-injected TE-NMI at 2 weeks post transplantation that was visualized following optical clearing and multiphoton microscopy. Robust TE-NMI neurons and axons (GFP) were found within the lumen protected from host cells entering the graft zone. (C–K) To assess whether TE-NMI axons extended in the otherwise denervated nerve and interacted with the Schwann cells, nerve cross-sections taken 5 mm distal to the transplant site were labeled for TE-NMI axons (GFP), Schwann cells (S100 β), nuclei (Hoechst; HST), and C-Jun (a gene encoding for a pro-regenerative transcription factor that is transiently found in denervated Schwann cells). (C) High resolution image showing an example of GFP + TE-NMI axons extending through aligned Schwann cells resembling the bands of Büngner. (D–E) Greater GFP outgrowth per nerve was found distal to two TE-NMIs than one TE-NMI. (F) At higher magnification, Schwann cells were readily observed with a subpopulation expressing C-Jun. (G) Greater number of cells was found in the 2x TE-NMI cohort compared to the acellular group. (H) Elevated C-Jun expression was also observed distal to two TE-NMIs. (I) Greater number of Schwann cells (identified by HST + S100 β co-localization) was also found in the 2x TE-NMI group. (J) A significant number of Schwann cells also co-localized with C-Jun distal to two TE-NMIs. These findings suggest TE-NMIs can interact with and potentially influence the host S100+ Schwann cells in the denervated distal nerve at 6 weeks post transplantation in a model of host nerve axotomy, as well as potentially preserve the pro-regenerative phenotype as evidenced by the C-Jun localization. Error bars represent standard error. Mean values compared using a one-way ANOVA followed by Tukey's post-hoc test. * $p < 0.05$. Scale bars: (C) 100 μm , (D) 100 μm , (E) 5 μm .

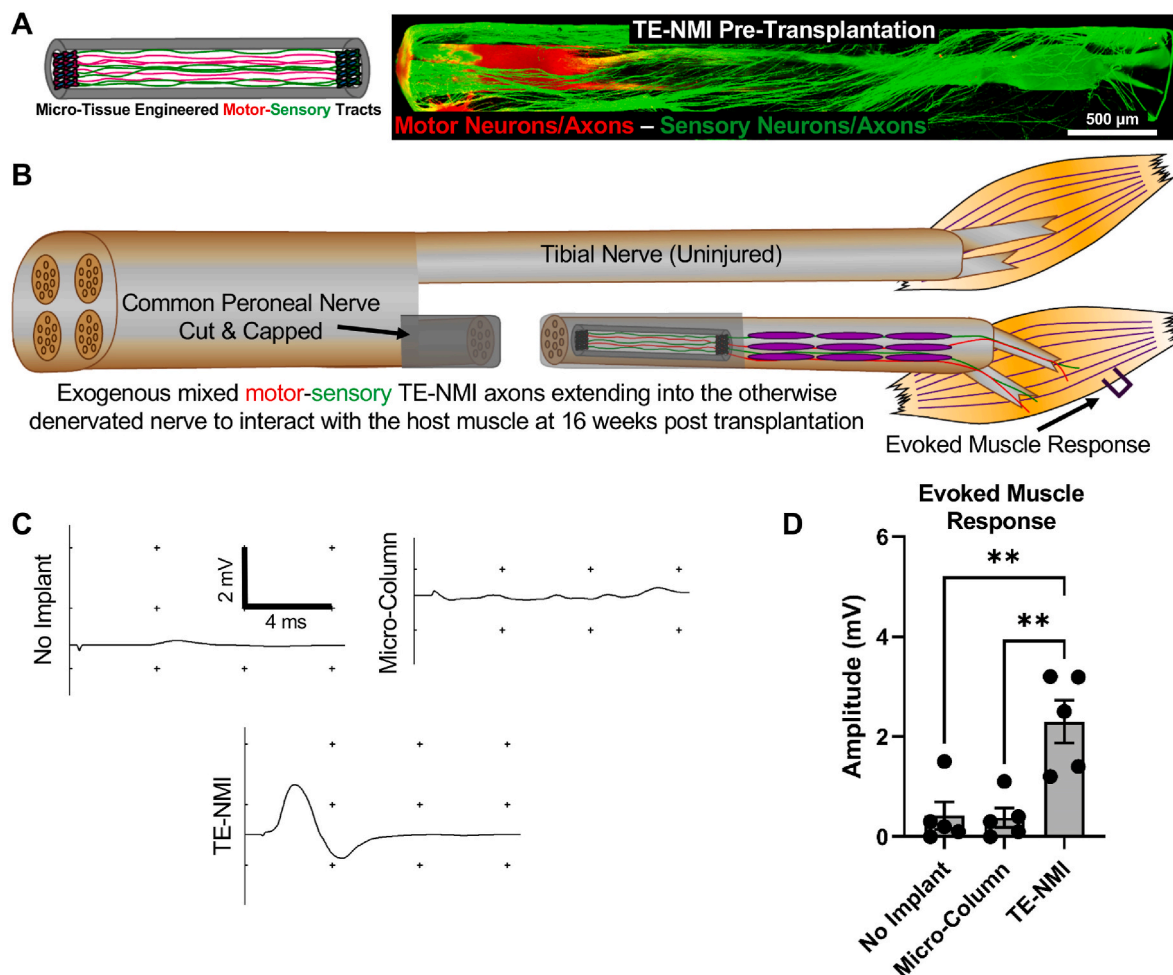
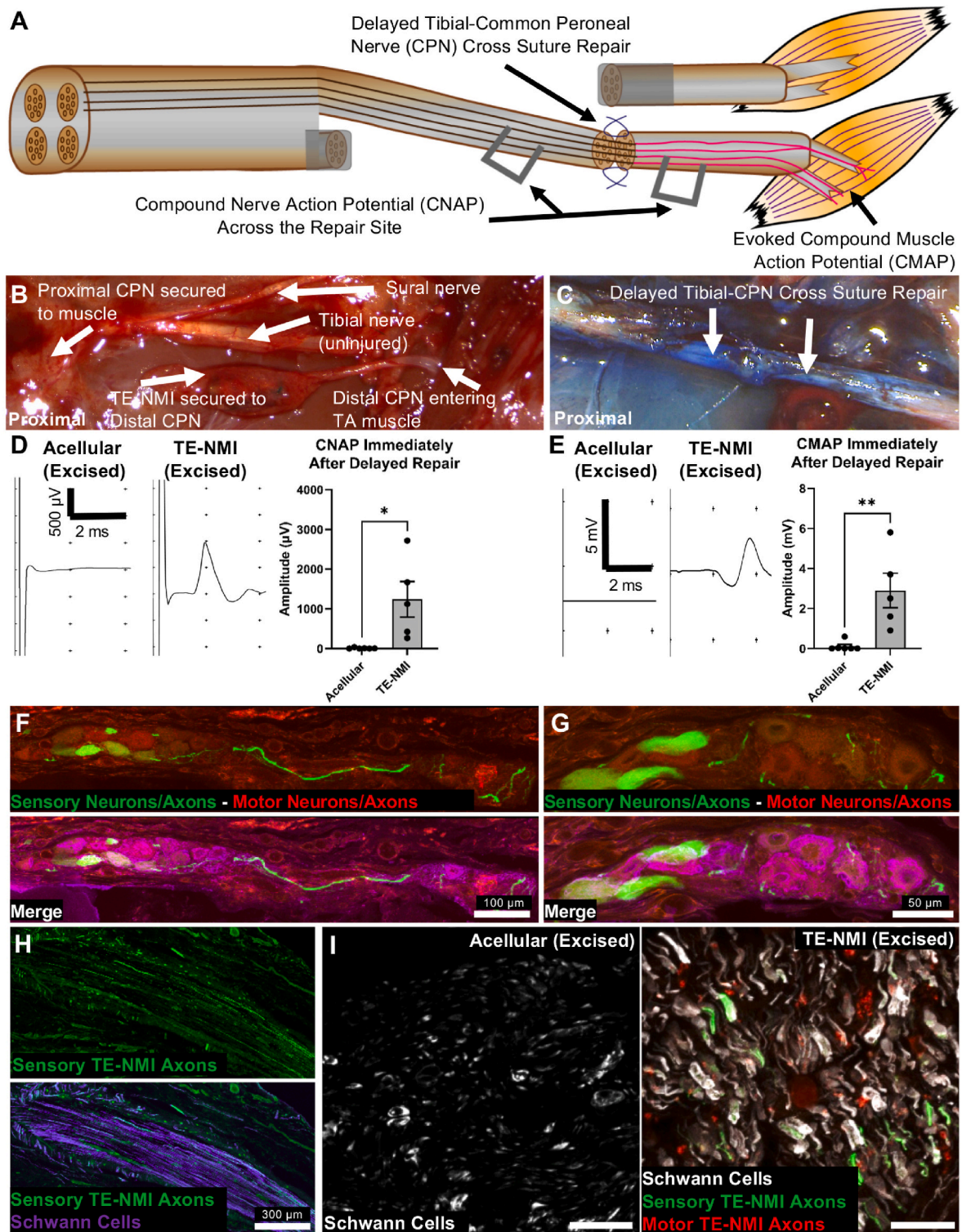


Fig. 3. Evoked Muscle Response at 16 Weeks Following TE-NMI Transplantation in Chronic Host Nerve Axotomy Model. (A) Representative confocal image of a mixed motor-sensory TE-NMI containing neuron populations transduced to express TD-tomato (motor, red) or GFP (sensory, green). (B) Schematic illustrating the surgical model, transplantation paradigm, and outcome measure. Mixed motor-sensory TE-NMIs were secured to the common peroneal nerve in a model of host chronic nerve axotomy. At 16 weeks post transplantation, the evoked muscle response was recorded following percutaneous stimulation over the common peroneal nerve innervating the distal target tibialis anterior muscle. (C) Compared to the irregular/lack of recordable waveform in the no implant or micro-column only control groups, a reproducible robust waveform was elicited in the TE-NMI group. (D) Greater mean amplitude of the evoked muscle response was found in the TE-NMI group compared to the controls. These findings suggest that TE-NMIs functionally integrate with the denervated muscle and preserve the electrophysiological muscle response at 16 weeks post chronic nerve axotomy. Error bars represent standard error. Mean values compared using a one-way ANOVA followed by Tukey's post-hoc test. ** $p < 0.01$.

extending within the otherwise denervated nerve that subsequently integrated with the muscle would be compatible for axon fusion following the standard PEG fusion protocol. At 20 weeks following TE-NMI transplantation, the distal nerve was freshly axotomized for nerve

fusion by excising the TE-NMI (Fig. 4A, B). To test whether TE-NMI transplantation enabled delayed fusion and promoted functional recovery, a cross-suture repair was utilized to avoid the need for grafting between the contracted proximal and distal stumps and minimizing



(caption on next page)

Fig. 4. Freshly-Cut TE-NMIs Axons in the Otherwise Denervated Distal Nerve Enable an Immediate Evoked Response Following Nerve Fusion. (A) Schematic illustrating the surgical model, delayed nerve fusion paradigm, and outcome measure. At 20 weeks post transplantation and host chronic nerve axotomy, the TE-NMI was removed leaving behind freshly transected axons in the distal nerve. To enable axon fusion, the graft was excised in hypotonic saline containing a calcium chelating agent, similar to previous protocols. (B) Intraoperative image at 20 weeks post transplantation showing the proximal common peroneal nerve secured to a nearby muscle, the TE-NMI secured to the distal nerve, and the uninjured tibial nerve coursing above it. (C) Intraoperative image immediately after delayed nerve repair showing the previously uninjured tibial nerve sutured to the distal portion of the common peroneal nerve following TE-NMI excision. The blue staining is due to methylene blue application during the fusion protocol. (D) Compound nerve action potentials recorded immediately after delayed nerve fusion were obtained in all animals that had received a TE-NMI. Greater nerve conductivity was found in the TE-NMI group compared to acellular controls. (E) Compound muscle action potentials were recorded after eliciting an evoked muscle response by stimulating proximal to the repair site. Greater evoked muscle response was observed in the TE-NMI group compared to acellular controls. (F) At 20 weeks post repair, the surgical site was re-exposed and the TE-NMI transplant was harvested for histological analyses. Representative longitudinal images are shown labeling neurons and dendrites with MAP2 (far red) and sensory and motor TE-NMI neurons and axons with endogenous expression of GFP and tdTomato, respectively. Robust TE-NMI neuron survival was found within the lumen at 20 weeks post transplantation. (G) At high magnification, healthy neurons were readily visualized within the micro-column co-labeling with MAP2. (H) Representative longitudinal nerve sections and (I) axial nerve cross-sections immediately distal to the excised transplant are shown labeled for Schwann cells (S100). Robust TE-NMI sensory outgrowth (GFP, green) was visualized. TE-NMI outgrowth was found (TD-Tomato, red), but the expression was weaker. Error bars represent standard error. Mean values compared using two-tailed unpaired Student's t-tests. * $p < 0.05$; ** $p < 0.01$. Scale bars: (F) 25 μm .

confounds associated with prolonged proximal neuron injury similar to the model previously described by Fu and Gordon [9].

Prior to performing the PEG fusion protocol using distal nerve segments re-populated with TE-NMI axons, we initially validated this cross-nerve fusion protocol using naïve proximal tibial nerve and naïve distal common peroneal nerve immediately following transection of each nerve. First, robust compound nerve action potentials (CNAPs) were measured across the naïve common peroneal nerve prior to transection (Fig. S2, top). Next, after transection and performing the cross-suture repair using the proximal tibial nerve and distal common peroneal nerve, clear CNAPs were obtained by stimulating the tibial nerve and recording from the common peroneal nerve only when the PEG fusion protocol was performed (Fig. S2, middle).

This cross-suture repair was then performed using animals that had previously received TE-NMIs by securing the proximal stump of the tibial nerve to the distal end of the common peroneal nerve containing TE-NMI axons (Fig. 4C), immediately following transection of each nerve. Electrical conduction was recorded immediately following this delayed nerve fusion in all TE-NMI animals compared to none of the controls (Fig. 4D). The mean CNAP amplitude of the TE-NMI group was $1240 \pm 1001 \mu\text{V}$ whereas the mean value for the acellular controls was $9.09 \pm 14.16 \mu\text{V}$ ($t = 3.045$, $df = 9$; $p = 0.0139$), suggesting the electrical conduction spanned the repair site and elicited a CNAP via the exogenous TE-NMI axons. Similarly, greater evoked muscle responses were recorded in the TE-NMI cohort following proximal stimulation (Fig. 4E). Here, to assess whether the exogenous axons could elicit an evoked muscle response, the proximal nerve stump was stimulated and recording electrodes were placed over the distal muscle belly. The mean amplitude of the evoked muscle response for the TE-NMI group was $2.9 \pm 1.93 \text{ mV}$, which resulted in approximately a 30-fold increase compared to the acellular controls ($0.1 \pm 0.24 \text{ mV}$; $t = 3.55$, $df = 9$; $p < 0.01$). Notably, no electrophysiological response was obtained after a delayed nerve repair was completed following TE-NMI transplantation without PEG application (Fig. S2, bottom), corroborating our previous findings demonstrating PEG is necessary for electrical conduction [34]. These electrophysiological findings suggest immediately after nerve repair, exogenous TE-NMI axons were suitable for the PEG nerve fusion protocol at a delayed time point. Moreover, within the harvested transplant site, robust TE-NMI neuron survival was visualized within the micro-column at 20 weeks post repair (Fig. 4F, G). Immediately distal to the excised transplant, no host axons were visualized (as expected), but sensory and motor axons fluorescently transduced prior to transplantation were observed extending from the TE-NMI neurons into the host distal nerve (Fig. 4H, I).

2.5. TE-NMIs enable greater electrophysiological recovery, axon maturation, and muscle reinnervation following delayed nerve repair

At 1 month post delayed nerve fusion (i.e. 24 weeks after initial

nerve transection), greater nerve and muscle electrophysiological functional recovery was found in the TE-NMI group (Fig. 5B, C). The mean CNAP amplitude at 1 month following delayed repair for the TE-NMI group was $460.9 \pm 306.50 \mu\text{V}$ and the acellular group was $43.3 \pm 58.60 \mu\text{V}$ ($t = 2.992$, $df = 8$; $p = 0.0173$). Faster conduction velocity was also found in animals that had previously received a TE-NMI prior to delayed nerve repair ($14.7 \pm 2.94 \text{ m/s}$) compared to the acellular controls ($8.5 \pm 2.22 \text{ m/s}$; $t = 4.004$, $df = 9$; $p = 0.0031$). At this early time point, an elevated evoked response was recorded from the distal muscle following stimulation in the TE-NMI group ($0.049 \pm 0.0305 \text{ mV}$) compared to the acellular group ($0.003 \pm 0.0055 \text{ mV}$; $t = 3.676$, $df = 8$; $p = 0.0063$). These data indicate at 1 month post delayed nerve repair, the TE-NMI group had greater electrophysiological recovery, including nerve conductivity and muscle reinnervation compared to the acellular controls.

To assess regeneration at 1 month post delayed repair, cross-sectional nerve morphometric analyses was completed to identify Schwann cells, host/fused axons, and myelin (Fig. 6A). At this time point, similar levels of SMI35 expression (i.e. total number of axons) were found distal to the repair site in the TE-NMI cohort (TE-NMI: $58.3 \pm 8.03\%$, acellular: $45.1 \pm 32.19\%$; $t = 0.7943$, $df = 7$; $p = 0.4531$; Fig. 6B). However, the mean area of the SMI35+ regions, a surrogate marker for axon size, was significantly greater in the TE-NMI group than the controls (TE-NMI: $107.9 \pm 14.76 \mu\text{m}^2$, acellular: $58.1 \pm 36.38 \mu\text{m}^2$; $t = 2.546$, $df = 7$; $p = 0.0383$; Fig. 6C). Often larger axon caliber indicates increased degree of axonal maturation, which typically accelerates following synapse formation with the end target and cessation of the axonal growth phase. An increased number of myelinated axons was also observed in the TE-NMI cohort (TE-NMI: 265.3 ± 65.54 myelinated axons, acellular: 135.0 ± 88.69 myelinated axons; $t = 2.546$, $df = 7$; $p = 0.0383$; Fig. 6D). Greater Schwann cell (S100 β +) expression was also found distal to the repair site in the TE-NMI group compared to acellular controls (TE-NMI: $15.25 \pm 5.01\%$, acellular: $6.91 \pm 4.70\%$; $t = 2.480$, $df = 7$; $p = 0.042$; Fig. 6E). At 1 month post delayed nerve fusion, muscle cross-sections were stained for acetylcholine receptors (bungarotoxin) to identify the neuromuscular junctions (NMJs) and synaptophysin, a presynaptic marker (Fig. 6F). Although no significant difference in the total number of acetylcholine receptors (AChR) were found in the target muscle (TE-NMI: 80.5 ± 47.59 AChR counts per area, acellular: 84.6 ± 49.76 AChR counts per area; $t = 0.1251$, $df = 7$; $p = 0.904$; Fig. 6G), a greater percentage of mature NMJs co-labeling AChR and synaptophysin were observed following TE-NMI transplantation (TE-NMI: $80.7 \pm 18.67\%$, acellular: $30.7 \pm 26.91\%$; $t = 3.141$, $df = 7$; $p = 0.016$; Fig. 6H). Further, elevated muscle weight was found in the TE-NMI group compared to the controls (data not shown). Collectively, these findings corroborate the electrophysiological data suggesting that TE-NMI transplantation preserves the pro-regenerative capacity of the otherwise denervated structures and ultimately accelerates host axon regeneration, maturation, and reinnervation following delayed nerve repair.

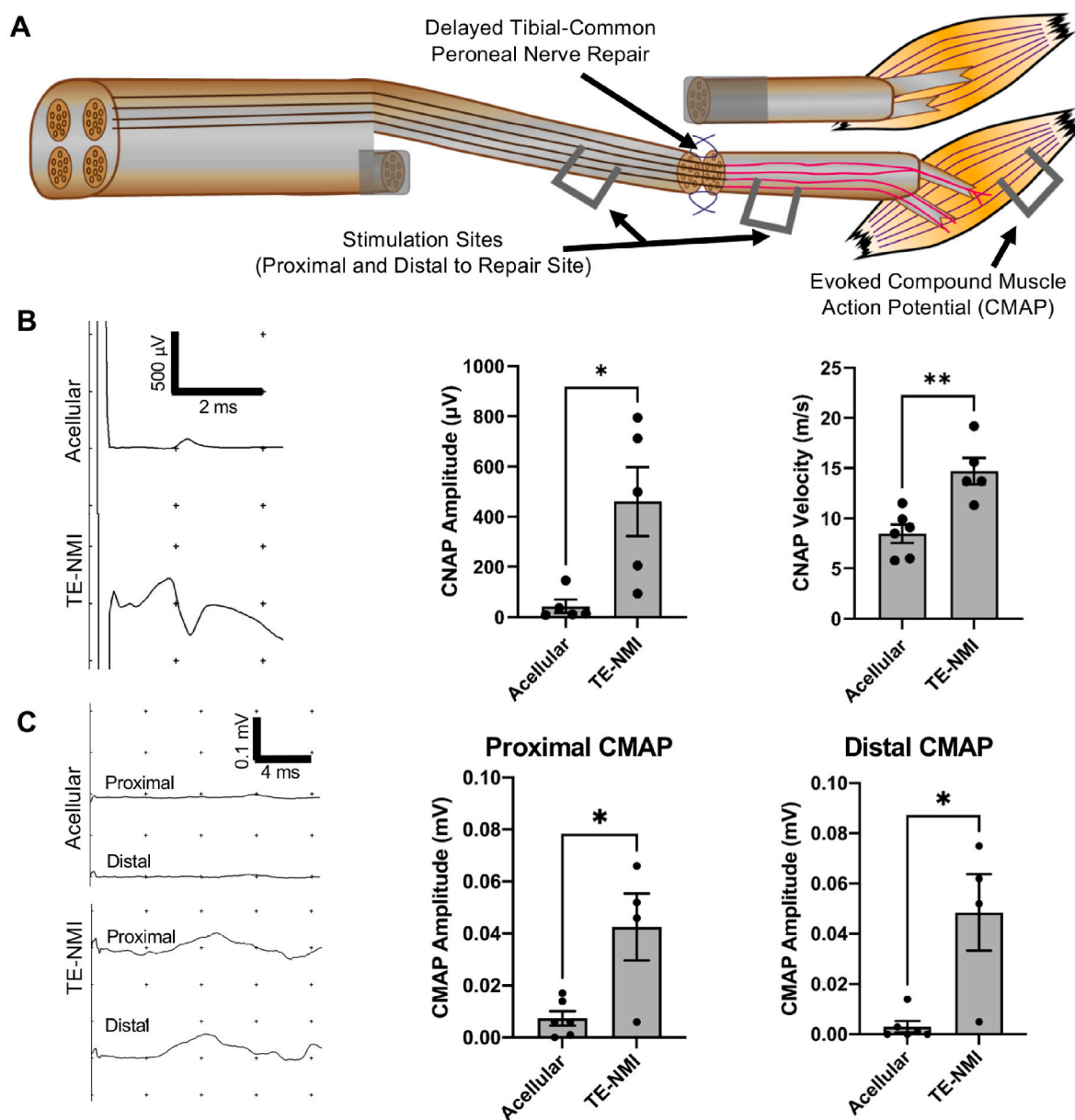
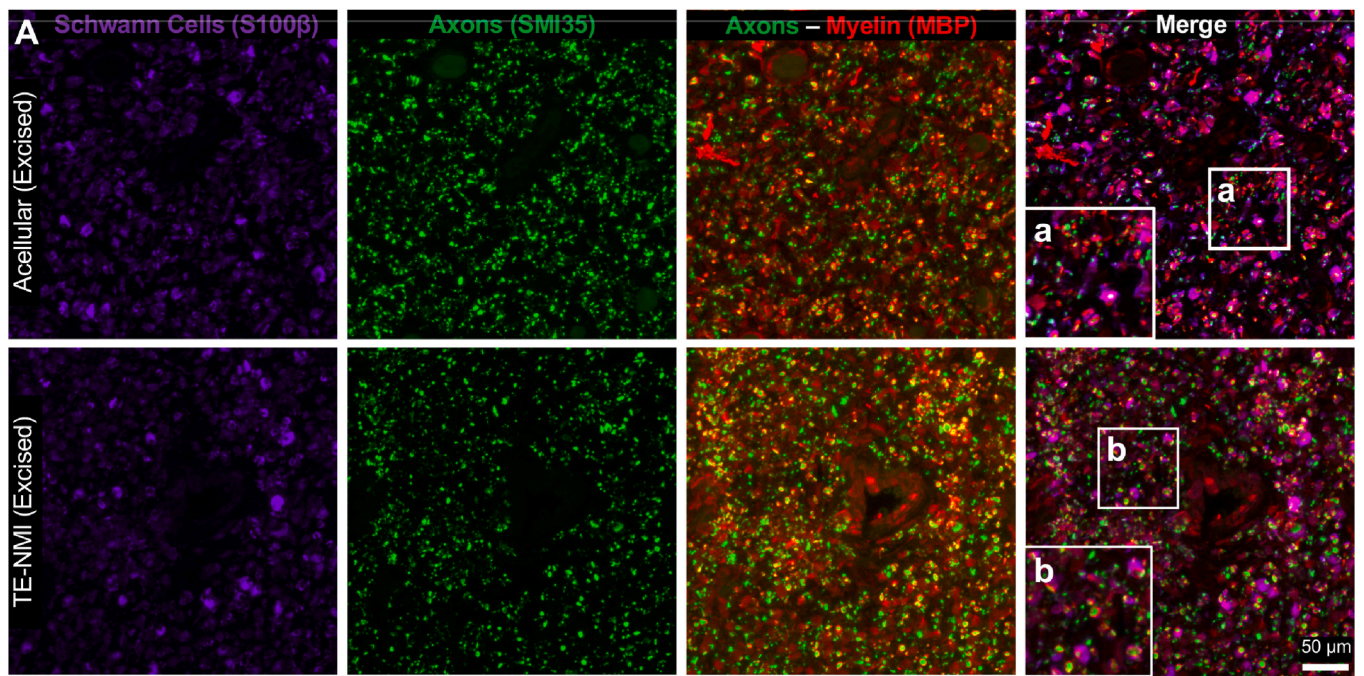


Fig. 5. Electrophysiological Functional Recovery at 1 Month Following Delayed Nerve Repair. (A) Schematic illustrating the electrophysiological outcome measures obtained at 1 month following delayed nerve repair (24 weeks following initial nerve transection). (B) Compound nerve action potentials (CNAPs) were elicited in both groups, however, a greater response and faster conduction velocity was observed in animals that had previously received a TE-NMI transplant. (C) Compound muscle action potentials (CMAPs) were recorded in all animals with an elevated evoked response in the TE-NMI group. Mean values compared using two-tailed unpaired Student's t-tests. Error bars represent standard error. * $p < 0.05$; ** $p < 0.01$.

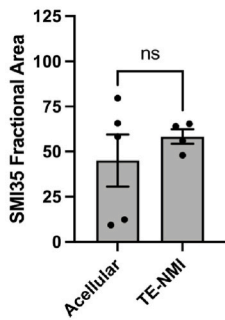
3. Discussion

In this study, TE-NMIs were developed as a novel implantable microtissue featuring preformed neural networks comprised of discrete populations of motor and sensory neurons spanned by bundled axonal tracts. Following implantation into transected rat nerve, we found that TE-NMI neurons extended numerous axons deep within the host tissue that closely interacted with the endogenous bands of Büngner and resulted in a greater Schwann cell response compared to controls. In addition, we showed that TE-NMI implants promoted nerve and muscle electrophysiological recovery following delayed nerve repair by preserving the pro-regenerative environment in the distal nerve. Collectively, we report TE-NMIs as the first engineered microtissue designed to prevent the harmful effects of prolonged denervation by providing a source of local axons to innervate the otherwise denervated muscle.

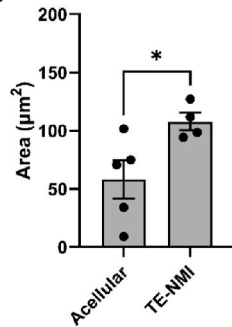
Although slow axon regeneration (1–2 mm/day) is often described as the main challenge for successful functional recovery after nerve injury, two additional important and often underappreciated factors are (1) the capacity for Schwann cells to support the injured proximal neurons and facilitate axon re-growth and (2) the receptiveness of the distal muscle for reinnervation [9,35]. A prolonged period of time without axon contact in the distal nerve and muscle is a common clinical occurrence, and often occurs in cases of delayed nerve repair, repair of proximal nerve injuries, and/or repair of long-gap nerve injuries. In these cases, prolonged denervation results in the loss of the pro-regenerative environment and target muscle receptiveness necessary for successful regeneration and reinnervation. Several regenerative-associated genes, transcription factors, and proteins are negatively impacted by prolonged denervation [36,37]. Immediately after injury, Schwann cells dedifferentiate and form pro-regenerative bands of Büngner; however, this



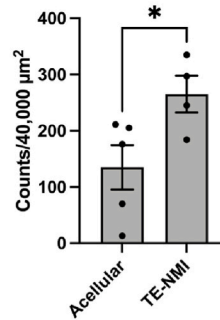
B SMI35 Expression



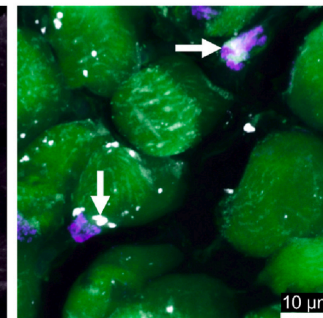
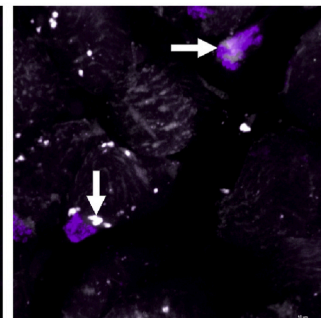
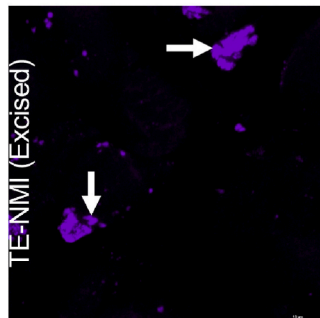
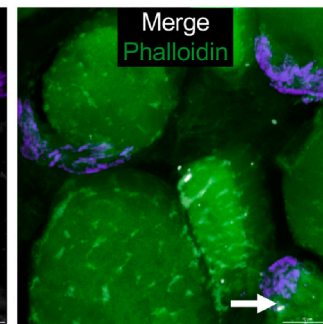
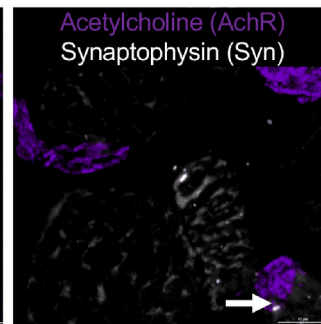
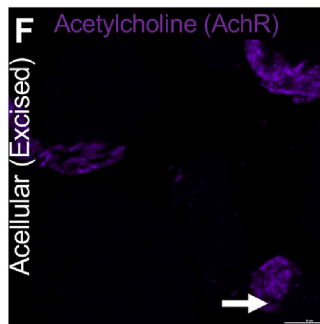
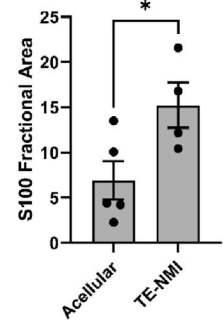
C Mean Axon Size



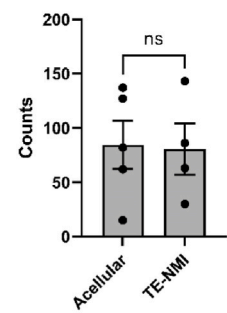
D Myelinated Axon Density



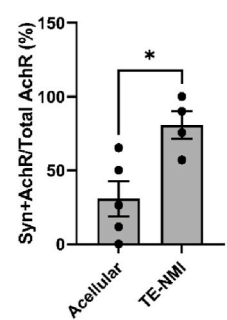
E S100β Expression



G Mean AChR Count



H Mean Mature NMJ



(caption on next page)

Fig. 6. Nerve Morphometry and Muscle Reinnervation at 1 Month Following Delayed Nerve Repair. (A) Representative confocal images of nerve cross-sections 5 mm distal to the repair site were labeled for Schwann cells (S100), host axons (SMI35), and myelin (myelin basic protein; MBP). (B) No differences in SMI35 expression were detected distal to the repair site, suggesting a comparable number of host axons regenerated into the distal sheath. (C) The mean area of SMI35+ regions found distal to the repair was greater in the TE-NMI cohort, indicating the host axons in the distal nerve were larger than the controls. (D) Greater number of myelinated axons were found distal to the repair in the TE-NMI cohort. (E) Increased S100 β expression, a common marker of Schwann cells, was observed in the TE-NMI group. (F) Representative confocal images of the tibialis anterior (TA) muscle cross-section stained for acetylcholine receptors (bungarotoxin) to identify the neuromuscular junctions (NMJs) and synaptophysin, a presynaptic marker (gray-scaled). Sections were counterstained with phalloidin to visualize muscle fibers. (G) No significant difference in the total number of AchR counts between groups. (H) Greater muscle reinnervation, as indicated by the percent of mature NMJ co-labeled for AchR and synaptophysin, was found in animals that previously received a TE-NMI transplantation. Collectively, these findings suggest that both while both groups are exhibiting ongoing regeneration, TE-NMIs may enable earlier axon maturation and muscle reinnervation following delayed nerve repair. Fractional area was calculated by measuring the percent area of positive fluorescent expression per ROI averaged over three ROIs. Mean values compared using two-tailed unpaired Student's t-tests. Error bars represent standard error. * $p < 0.05$; ** $p < 0.01$.

transient phenotype eventually degrades due to the lack of axonal contact. Indeed, in this study, the total number of cells in the distal nerve at 6 weeks following axotomy was ~ 1.5 x greater in the cohort receiving 2 TE-NMI implants compared to the acellular controls. On closer examination of these cells, there was a ~ 1.7 -fold increase in co-expression of S100 β in the distal nerve following 2 TE-NMI implants compared to controls. Moreover, 2 TE-NMI implants also led to an ~ 1.5 -fold increase in Hoechst+, S100 β +, C-Jun + cells that were observed in distal nerve. These data corroborate previous findings suggesting C-Jun expression is pro-regenerative and is rapidly elevated in Schwann cells after injury to promote axonal regeneration and motor neuron survival [38–40]. Moreover, our data suggest an adequate “dose” of TE-NMI may be necessary to preserve the pro-regenerative Schwann cell phenotype in a rodent model of prolonged denervation. Interestingly, there was more than a 2-fold increase in total C-Jun expression following transplantation of 2 TE-NMIs compared to controls (although not necessarily always in Hoechst+, S100 β + cells), which suggests TE-NMIs may be modulating other cells in the distal nerve. Future work is necessary to further elucidate the underlying mechanism-of-action and to potentially determine the optimal dosage requirement per fascicle.

To date, there are no commercially available strategies designed to “babysit” or preserve the regenerative capacity of the distal nerve. Innovative surgical techniques have been proposed, such as supercharged end-to-side (SETS) nerve transfers that reroute axons into the denervated distal nerve distal to the primary repair and generally much closer to the end target [41]. Indeed, SETS may improve functional recovery in challenging nerve repairs by enabling early reinnervation with axons far afield (more distal) to the primary repair site [42–44]. However, nerve transfers are only indicated in specific scenarios, require transection of an otherwise healthy nerve, and increase the risk for painful neuroma formation. Therefore, TE-NMIs may be more desirable as a broadly applicable tissue engineering-based approach to “babysitting” that preserves the regenerative capacity of the Schwann cells in the distal nerve as well as target muscle without deliberately transecting an otherwise healthy nerve.

TE-NMIs are the first preformed neuron-axonal microtissue designed to improve functional recovery following nerve repair. These efforts build on previous studies that have shown ectopic neurons transplanted in the distal nerve may preserve the regenerative capacity of the Schwann cells and muscle, and promote functional recovery following delayed nerve repair [45–48]. In addition, previous work by our group has shown that tissue engineered nerve grafts (TENGs), a stretch-grown living scaffold comprised of neurons and long axonal tracts, also extend neurite processes into the otherwise denervated nerve [49]. TENGs simultaneously facilitate axon regeneration across challenging defects while preserving the regenerative capacity within the distal nerve [33]. While this dual mechanism remains promising for bridging repairs, transplantation requires nerve transection, which for distal nerve babysitting would require disruption of the otherwise intact distal nerve architecture. Therefore, TE-NMIs were developed as a next-generation babysitting strategy that is amenable for minimally invasive delivery. Indeed, we have shown that TE-NMI axons can extend at least 5 mm within the otherwise denervated distal stump and promote Schwann cell

expression at 6 weeks following transplantation. However, future studies are necessary to characterize the rate of TE-NMI axonal extension post transplantation and determine the optimal window for delivery.

Nerve fusion has been well described by Bittner and others as a novel approach that immediately restores axon membrane continuity and electrical conduction across coaptation site(s) following repair [10–20]. These studies also report that nerve fusion – when performed acutely after nerve injury – prevents Wallerian degeneration, minimizes muscle atrophy, and promotes reinnervation, which collectively result in rapid behavioral recovery. While the prospect of nerve fusion remains exciting, it is currently limited to acute nerve injury due the progression of Wallerian degeneration, resulting in distal axon breakdown that prohibits fusion. In this study, we show the first example of delayed nerve fusion using exogenous TE-NMI axons in the otherwise denervated distal sheath. After demonstrating TE-NMI transplantation preserves the evoked muscle response up to 20 weeks post injury/transplantation, we tested whether TE-NMI axons in the distal stump were amenable for delayed fusion. We hypothesized that TE-NMI axotomy within hypotonic saline, calcium chelator, and then PEG would temporarily prevent axon sealing and enable delayed nerve fusion. Our findings suggest that fusion was achieved by sacrificing the TE-NMI somata, potentially allowing for immediate connection with the freshly axotomized distal exogenous axons and host axons in the proximal stump. After completing the fusion protocol, the TE-NMI cohort showed immediate nerve action potentials conducted across the repair site and an evoked muscle response following either proximal stimulation (i.e. stimulating tibial axons potentially fused with distal TE-NMI axons within the common peroneal) or distal stimulation (i.e. stimulating distal TE-NMI axons directly) compared to the control groups lacking exogenous axons. However, it is important to note that by 1 month following the delayed fusion protocol, the actual percentage of host axons fused to distal TE-NMI axons remains unknown, although a large number of unfused TE-NMI axons likely fully completed Wallerian degeneration. Moreover, even acutely fused axons may be inherently unstable and a significant proportion may undergo delayed Wallerian degeneration. In any scenario, it is difficult to distinguish regenerating host axons from successfully fused axons; however, the majority of axons in the distal nerve segment are likely regenerating from the proximal stump and actively undergoing maturation and reinnervation of the previously denervated muscle, as shown histologically with increased axon size and number of myelinated axons in the fused TE-NMI animals. At 1 month post fusion, although greater electrophysiological recovery was seen in the TE-NMI cohort compared to the acellular controls, there was a stark decrease compared to the initial recovery, which may be explained by Wallerian degeneration of unfused axons or pruning of fused axons during the maturation process. Future mechanistic studies may be helpful in understanding the beneficial effects of preventing prolonged denervation and determining the optimal window for delayed nerve fusion using exogenous axons.

In this study, the hydrogel encasement was designed to protect the neuronal/axonal cargo following transplantation. Several cell transplantation strategies are currently being investigated, including human

iPSC-derived neurons. Here, we tested the efficacy of TE-NMIs comprised of allogenic rodent embryonic neurons as proof-of-concept. However, it remains unclear whether immunosuppression would be necessary if TE-NMIs were fabricated from a clinically-relevant starting cell source. Therefore, additional testing using a human-compatible starting cell source, such as human iPSC-derived neurons, is necessary in immunocompetent and immunocompromised preclinical models. For example, human iPSC-derived TE-NMIs may be tested in a clinically-relevant rodent or porcine models of nerve injury to determine the effects of immunosuppression on babysitting and axon fusion phenomenon [34,50].

This work complements previous studies demonstrating the importance of restoring early reinnervation following nerve injury. Moreover, innervation plays an important role in development and has been shown to be crucial during the biofabrication process of tissue engineered end-organ or muscle scaffolds [51]. Moreover, future work may include using TE-NMIs as an adjunctive strategy to augment tissue biofabrication or for other regenerative strategies requiring exogenous axons, such as volumetric muscle loss or spinal cord injury [30,51,52].

Based on these findings, TE-NMIs may represent a transformative approach for restorative peripheral nerve surgery that allows for exogenous axons to provide early muscle reinnervation for enhancing the likelihood for successful recovery following delayed nerve repair. Moreover, the exogenous axons may potentially be spliced in with the host nerve, thus enabling delayed nerve fusion. With further development, TE-NMIs may offer surgeons an opportunity to improve functional recovery and restore hope for patients with injuries not currently amenable for nerve transfer.

4. Methods

All procedures were approved by the Institutional Animal Care and Use Committees at the University of Pennsylvania and the Michael J. Crescenz Veterans Affairs Medical Center and adhered to the guidelines set forth in the NIH Public Health Service Policy on Humane Care and Use of Laboratory Animals (2015).

4.1. Embryonic neuron isolation and spinal motor aggregation

Spinal cords and dorsal root ganglia (DRG) were isolated from embryonic day 16 Sprague-Dawley rats (Charles River, Wilmington, MA) as previously described. DRG explants were stored overnight in Hibernate-E and were transduced with AAV2/1.hSynapsin.EGFP.WPRE.bGH (UPenn Vector Core). Motor neuron aggregates were formed following force-aggregation of spinal motor neurons isolated from dissociated spinal cords using an Optiprep density gradient as previously described. Motor neuron aggregates were incubated overnight in media and were transduced with an AAV.hSynapsin.tdTomato vector. Neurons were plated in spinal astrocyte-conditioned Neurobasal media +10% FBS supplemented with 37 ng/mL hydrocortisone, 2.2 µg/mL isobutylmethylxanthine, 10 ng/mL BDNF, 10 ng/mL CNTF, 10 ng/mL CT-1, 10 ng/mL GDNF, 2% B-27, 20 ng/mL NGF, 20 µM mitotic inhibitors, 2 mM L-glutamine, 417 ng/mL forskolin, 1 mM sodium pyruvate, 0.1 mM β-mercaptoethanol, 2.5 g/L glucose [31].

4.2. Micro-column fabrication

Agarose or agarose-gelatin hydrogels micro-columns were constructed using a three-phase process similar to methods previously described [28–30,32]. Briefly, agarose micro-columns were formed using glass capillary tubes (345–701 µm) allowing for the insertion of acupuncture needles (180–350 µm) through the lumen. Molten agarose (3% weight/volume) in Dulbecco's phosphate buffered saline (DPBS) was added to the capillary tube containing the acupuncture needle and allowed to cool. The acupuncture needle was quickly removed to create the hydrogel shell, and the micro-columns were stored in DPBS at 4 °C.

Agarose-gelatin micro-columns (1.5% agarose+1.5% gelatin) were fabricated as described above except that micro-columns were stored in 7 mL DPBS with 100 µl at room temperature overnight and subsequently washed 3 times in DPBS prior to further experiments. All micro-columns were cut to the appropriate length, UV sterilized for 30 min, and stored in DPBS at 4 °C.

Micro-columns were transferred to a new Petri dish and excess DPBS was removed from the lumen of the micro-column via micropipette and replaced by extracellular matrix (ECM), comprised of 1.0 mg/mL rat tail collagen + 1.0 mg/mL mouse laminin (Reagent Proteins, San Diego, CA). DRG explants or motor neuron aggregates were carefully placed at the ends of the micro-columns containing ECM, under stereoscopic magnification using fine forceps and were allowed to adhere for 45 min at 37 °C, 5% CO₂. Sensory TE-NMIs were generated by seeding a DRG explant on each end of a micro-column. Motor TE-NMIs were created by seeding a motor neuron aggregate on each end of a micro-column. Mixed motor-sensory TE-NMIs were fabricated by seeding a motor neuron aggregate and a DRG explant on opposite ends of a micro-column. TE-NMIs were then returned to culture and allowed to grow with fresh media replacements every other day.

For mixed TE-NMI characterization, prior to plating, motor neurons were transduced overnight to endogenously express GFP and sensory neurons were transduced overnight to endogenously express tdTomato. For the rest of the *in vitro* characterization and *in vivo* implementation, motor neurons were transduced overnight with tdTomato and sensory neurons were transduced overnight with GFP. All TE-NMIs were returned to culture following fabrication with half media changes every other day.

4.3. Immunocytochemistry

TE-NMIs were fixed in 4% paraformaldehyde for 35 min, rinsed in 1x PBS, permeabilized with 0.3% Triton X100 + 4% horse serum in PBS for 60 min, and then incubated with primary antibodies overnight at 4 °C. Primary antibodies were Tuj-1/beta-III tubulin (T8578, 1:500, Sigma-Aldrich) to label axons and synapsin-1 (A6442, 1:500, Invitrogen) to label pre-synaptic specializations. Following primary antibody incubation, TE-NMIs were rinsed in PBS and incubated with fluorescently-tagged secondary antibodies (1:500; Invitrogen) for 2 h at 18°–24 °C. Finally, Hoechst (33342, 1:10,000, ThermoFisher) was added for 10 min at 18°–24 °C before rinsing in PBS. TE-NMIs were imaged on a Nikon A1RSI Laser Scanning confocal microscope paired with NIS Elements AR 4.50.00. Sequential slices of 10–20 µm in the z-plane were acquired for each fluorescent channel. All confocal images presented are maximum intensity projections of the confocal z-slices.

4.4. *In vitro* TE-NMI imaging

Phase-contrast microscopy images of TE-NMI were taken over several days *in vitro* (DIV) to measure neurite length and calculate growth rates. TE-NMI viability and presence of the desired neuronal phenotype(s) were quantified. at 10x magnification using a Nikon Eclipse Ti-S microscope, paired with a QIClick camera and NIS Elements BR 4.13.00.

Confocal imaging of TE-NMIs were taken on a Nikon A1RSI Laser Scanning confocal microscope paired with NIS Elements AR 4.50.00. Sequential slices of 10–20 µm in the z-plane were acquired for each fluorescent channel. All confocal images presented are maximum intensity projections of the confocal z-slices.

4.5. Chronic rodent sciatic nerve axotomy and acute TE-NMI transplantation

The capability of TE-NMIs to integrate with the denervated distal nerve was evaluated in a rodent chronic axotomy model. Male Sprague-Dawley rats (Charles River Laboratories; 300–330 g; aged 6–8 weeks)

were anesthetized with isoflurane and the hind leg cleaned with betadine. Meloxicam (2 mg/kg) was administered subcutaneously in the scruff of the neck and bupivacaine (2 mg/kg) was administered subcutaneously along the incision. The gluteal muscle was separated to expose the sciatic nerve exiting the sciatic notch.

TE-NMIs (3 mm long) were transplanted in the distal nerve using three different surgical paradigms. In a proof-of-concept experiment, an intraneural TE-NMI transplantation was performed in a subset of animals to demonstrate TE-NMI survival following micro-injection. Briefly, the sciatic nerve was exposed as described above. The TE-NMI was loaded into a Hamilton syringe and deposited into the nerve. The epineurium of the sciatic nerve was carefully incised and the needle containing the TE-NMI was inserted into the exposed fascicle, advanced 7 mm into the nerve, and the TE-NMI was deposited within the nerve and the epineurium was closed with 8-0 prolene. The nerve was sharply transected, and the proximal stump was inserted in a nearby muscle. TE-NMI survival was assessed at 2 weeks post transplantation using tissue clearing and multi-photon microscopy.

To evaluate sensory TE-NMI outgrowth and Schwann cell expression within the otherwise denervated distal nerve, a 5 mm segment of the sciatic nerve was excised, 5 mm proximal to the trifurcation, and the proximal nerve was capped with Teflon tape or secured to a nearby muscle. Sensory TE-NMI were placed in a 5 mm nerve wrap (Stryker Orthopedics, Kalamazoo MI) secured to the nerve to provide a protective environment for the nerve and TE-NMI. Approximately 100 μ l of 2 mg/mL collagen ECM was applied within the wrap to facilitate outgrowth of the TE-NMI axons in the distal nerve. Animals were randomly assigned to the following groups: (A) one sensory TE-NMI (n = 5); (B) two sensory TE-NMIs (n = 5), (C) acellular control micro-columns containing ECM only (n = 5).

To assess chronic integration with the otherwise denervated muscle, mixed motor-sensory TE-NMI were transplanted in a nerve wrap as described above. In this experiment, the common peroneal nerve was dissected to its proximal origin and the nerve was transected 5 mm distal to the bifurcation. The proximal common peroneal nerve stump was inserted in a nearby muscle. Mixed motor-sensory TE-NMI were placed in a 5 mm nerve wrap (Stryker Orthopedics, Kalamazoo MI) secured to the nerve to provide a protective environment for the nerve and TE-NMI. Approximately 100 μ l of 2 mg/mL collagen ECM was applied within the wrap to facilitate outgrowth of the TE-NMI axons in the distal nerve. Animals were randomly assigned to the following groups: (A) mixed TE-NMI (n = 5); (B) micro-column control (n = 5), (C) no implant control (n = 5).

In all procedures, the surgical site was closed with 4-0 absorbable vicryl sutures and skin staples. Animals were recovered and returned to the vivarium for the duration of the study.

4.6. Delayed axon fusion

At 20 weeks post transplantation and chronic axotomy, animals were anesthetized and the surgical site was re-exposed. The surgical site was irrigated with calcium free PlasmaLyte-A with a calcium chelating agent, the transplant was isolated and the distal common peroneal nerve was sharply transected. As the transected nerve was bathed with additional PlasmaLyte-A, the tibial nerve was sharply transected and a standard end-to-end nerve repair was completed using 2 8-0 prolene sutures, securing the proximal tibial nerve with the distal common peroneal nerve. Immediately before tightening the sutures, hypotonic 1% methylene blue solution was applied to the nerve ends, followed by administration of high molecular weight polyethylene glycol (3350 MW). Calcium-containing lactated ringer's solution was applied to the wound to wash away excess PEG. Electrophysiological recordings were performed immediately before and after repair to evaluate acute electrophysiological recovery as described below. The deep layers and skin were closed, and the area was dressed as described above. Prior to the delayed axon fusion study, the PEG fusion protocol was tested in naïve

rats (n = 2). Pre-injury and post-repair nerve action potentials were elicited by recording from the common peroneal nerve after stimulating the common peroneal nerve or tibial nerve, respectively (Fig. S2). Additionally, we also tested whether nerve conduction would span a repaired nerve following TE-NMI transplantation without PEG application (Fig. S2).

4.7. Immunohistochemistry

At the terminal time point, animals were euthanized with an intracardial injection of Euthasol. Nerves were extracted and post-fixed in formalin for 24 h at 4 °C, and then rinsed in PBS for another 24 h. Muscles were extracted in paraformaldehyde for 24 h at 4 °C and then cryoprotected in 20% sucrose.

For histological assessment following transplantation, the tissue was placed in 30% sucrose overnight, embedded in optimal cutting media, and then frozen in dry ice/isopentane. The transplant site was sectioned longitudinally and a region 5 mm distal to the transplant was sectioned axially at a thickness of 20 μ m, mounted on glass slides for staining. Frozen sections were washed three times in PBS, blocked and permeabilized in 4% normal horse serum with 0.3% Triton X-100 for 1 h. All subsequent steps were performed using blocking solution for antibody dilutions. Neurons were labeled with chicken anti-MAP2 (1:500, Abcam, ab532) and Schwann cells were labeled with anti-S100 β (1:500, Invitrogen, PA1-38585). Primary antibodies were applied overnight at 4 °C followed by the appropriate fluorophore-conjugated secondary antibody (1:1000; AlexaFluor, Invitrogen) for 2 h at room temperature. Hoechst was applied (1:10,000) prior to mounting with Fluoromount G and cover slipping. Sensory neurons/axons were visualized by the endogenous GFP expression and motor neurons by the endogenous tdTomato expression. Detailed morphometric analyses of the distal nerve was completed at 6 weeks post transplantation by labeling sections with guinea pig anti-S100 β (1:200, Synaptic Systems, 287 004) and rabbit anti-C-Jun (1:200, Cell Signaling Technologies, 9165 L), followed by appropriate application of AlexaFluor secondaries and Hoechst.

For cross-sectional histological assessment of the distal nerve following delayed nerve repair, a 1 cm segment of nerve distal to the repair zone was embedded in paraffin. The block was then mounted on a microtome and sectioned axially at a thickness of 8 μ m, mounted on glass slides, and prepared for staining as follows. Axial cross-sections were deparaffinized in xylene and rehydrated with a descending gradient of ethanol. Following rehydration, antigen retrieval was performed in TRIS/EDTA buffer for 8 min using a modified pressure cooker/microwave technique. Next, normal horse serum in Optimax (Biogenex) was applied to the sections (VectaStain Universal kit per manufacturer's instructions). Sections were incubated overnight at 4 °C with mouse anti-SMI35 to label axons (1:1000, Covance, SMI-35 R), rabbit anti-S100 β (1:500, Invitrogen, PA1-38585), and chicken anti-myelin basic protein (Encor, CPCA-MBP; 1:1500) in Optimax + normal horse serum (VectaStain Universal kit per manufacturer's instructions). After washing the sections three times for 5 min with PBS/TWEEN, the appropriate fluorophore-conjugated secondary antibody (1:1000; AlexaFluor, Invitrogen) was applied for 1 h at room temperature. After rinsing three times for 5 min with PBS/TWEEN, was applied for 20 min. Finally, sections were washed as above and cover slipped.

For muscle cross-sectional histological analyses, the tibialis anterior muscle was harvested and stored in 2% paraformaldehyde overnight. Muscles were cryoprotected in 20% sucrose overnight, blocked, frozen, sectioned axially at a thickness of 14 μ m, and stained following the protocol described above. Sections were incubated with rabbit anti-synaptophysin to identify presynaptic vesicles (1:500, Abcam, ab32127) at 4 °C overnight, followed by concurrent application for 2 h at room temperature of AlexaFluor-488-conjugated phalloidin (1:400, Invitrogen, A12379) to identify muscle actin, anti-rabbit AlexaFluor-568 (1:500, ThermoFisher, A10042) and AlexaFluor-647-conjugated bungarotoxin to identify postsynaptic receptors (1:1000, Invitrogen,

B35450).

4.8. Tissue clearing

A subset of nerves were extracted for tissue clearing using the Visikol protocol. Briefly, following fixation in formalin for 24 h at 4 °C, nerves were rinsed overnight with PBS at 4 °C, dehydrated in a series of ethanol washes for 2 h each (30%, 50%, 70%, and 90%) and 100% ethanol for 24 h. Next, nerves were incubated in Visikol 1 for 24 h followed by Visikol 2 for at least 24 h to complete the clearing process. TE-NMI survival within the graft region was visualized using multiphoton microscopy (Nikon).

4.9. Muscle and nerve electrophysiological assessment

At 16 weeks post axotomy, the evoked muscle response was compared across groups following percutaneous stimulation. Animals were re-anesthetized and a bipolar subdermal stimulating electrode was placed percutaneously superficial to the common peroneal nerve. A monopolar subdermal recording electrode was placed over the muscle belly of the tibialis anterior and the reference electrode placed in its tendon. The nerve was stimulated (biphasic; amplitude: 0–5 mA; duration: 0.2 ms; frequency: 1 Hz) using a handheld bipolar hook electrode (Rochester Electro-Medical, Lutz, FL; #400900). After determining the initial threshold for evoked muscle recordings, the supramaximal recording was obtained by slowly increasing the current to maximize the amplitude to double the threshold current or until the waveform plateaued, and then averaged over a train of 5 pulses (100x gain; 10–10,000 Hz band pass and 60 Hz notch filters; Natus Viking EDX). At 20 weeks post axotomy, animals were re-anesthetized and the surgical site was exposed for direct nerve stimulation and recordings. Compound muscle action potentials (CMAP) were assessed to evaluate the evoked muscle response following distal nerve stimulation (biphasic; amplitude: 0–4 mA; duration: 0.2 ms; frequency: 1 Hz; 1000x gain; 10–10,000 Hz band pass and 60 Hz notch filters; Natus Viking EDX). Proximal and distal CMAPs were recorded following delayed nerve repair by stimulating 5 mm proximal or distal to the repair site, respectively. Mean peak-to-baseline amplitude were recorded. To assess the immediate electrical conduction across the repair site, compound nerve action potentials (CNAP) were recorded by stimulating the proximal stump with a bipolar hook electrode and recording with a bipolar hook electrode (biphasic; amplitude: 0–2 mA; duration: 0.2 ms; frequency: 1 Hz; 1000x gain; 10–10,000 Hz band pass and 60 Hz notch filters; Natus Viking EDX). Mean peak-to-peak amplitude was recorded and conduction velocity was calculated by dividing the distance between the electrodes by the latency. At 1 month post delayed nerve repair (total 24 weeks following chronic host axotomy), CNAPs and CMAP recordings were obtained as described above.

4.10. Data acquisition and statistical analyses

Neuronal constructs were imaged using phase-contrast or epifluorescence microscopy on a Nikon Eclipse Ti-S with digital image acquisition using a QiClick camera interfaced with Nikon Elements Basic Research software (4.10.01). Fluorescent images were obtained with a Nikon A1R confocal microscope (1024 × 1024 pixels) with a 10x air objective and 60x oil objective using Nikon NIS-Elements AR 3.1.0 (Nikon Instruments, Tokyo, Japan). Multiple confocal z-stacks were digitally captured and analyzed, with all reconstructions tiled across the full section and full z-stack thickness.

For all TE-NMI neurite outgrowth assays, the longest neurite was measured from the edge of the aggregate ($n = 8–12$ TE-NMIs per condition at each time point). For TE-NMI fabrication characterization, mean neurite outgrowth was compared via a repeated two-way analysis of variance (ANOVA) with cell type and biomaterial hydrogel encasement as the two independent variables at 1 and 3 DIV.

All histological assessments were performed at the graft site (longitudinal frozen), 5 mm distal to the graft site (axial frozen), or 5 mm distal to the delayed nerve repair (axial paraffin). For frozen tissue, neurons were labeled with MAP-2, TE-NMI neurons/axons were identified as GFP + for sensory neurons/axons or tdTomato + for motor neurons/axons. For paraffin tissue, SMI35 labeled only the host regenerating/fused axons.

Distal nerve morphometry was assessed at 6 weeks post injury using an automated segmentation algorithm on three representative regions of interest (ROIs) per sample. Briefly, images were gray-scaled and filtered using a rolling ball background subtraction (size: 50 μm) and thresholded based on fluorescence and size (0.5 μm –20 μm). Objects were separated using a watershed algorithm and then quantified. Smaller particles and holes were removed from the binary mask using the “Clean” and “Fill Hole” functions (Nikon, NIS Elements). The total number of cells was quantified based on the Hoechst + nuclei. To quantify the number of S100 β + cells (Schwann cells), the binary layer function, “HAVING”, was used on the Hoechst and S100 β layers, yielding the number of Hoechst + cells expressing S100 β . After quantifying the C-Jun expression, the number of cells co-expressing S100 β and C-Jun was quantified using the HAVING function on the Hoechst + S100 β and C-Jun binary layers.

Myelinated axon counts were manually quantified by a blinded researcher from representative z-stacks at maximum projection of a 40,000 μm^2 region of interest at high magnification. All other axial nerve morphometry measurements were calculated from confocal z-stack maximum projections and analyzed using FIJI software [53]. Automated image processing macros were used to minimize any potential bias. Individual channels were isolated using MaxEntropy thresholding and subsequently quantified using the “Analyze Particles” function on features with an area greater than 1 μm^2 to minimize noisy signal. Total count of segmented particles, size of segmented particles, and the percent area covered was calculated from 2–3 sections per animal. Mean values were obtained by averaging the values per animal across groups for further statistical analyses.

For TE-NMI outgrowth and distal nerve analyses (i.e. Hoechst expression and co-localization with S100 β + Schwann cells and C-Jun) at 6 weeks post transplantation/host axotomy, mean values were compared by one-way analysis of variance (ANOVA) between the following groups: (a) one TE-NMI, (b) two TE-NMIs, (c) micro-column only. For the evoked muscle response at 16 weeks post transplantation/host axotomy, mean CMAP amplitude were compared by one-way ANOVA between the following groups: (a) TE-NMI, (b) micro-column only, and (c) injury only/no transplantation.

To quantify the total number of acetylcholine receptors (AChR) and percentage of mature neuromuscular junctions, a researcher blinded to the experimental groups first imaged each muscle section at low magnification to identify regions of bungarotoxin+ (BGX+) clusters of AChR (10x air objective, 1024 × 1024). Next, three regions of interest (ROI) were randomly selected and automatically acquired (2 × 2 region, 100x oil objective with a 2x digital zoom, 2048 × 2048) without the researcher visualizing the synaptophysin channel prior to acquisition. BGX + cells or the total number of AChR receptors were quantified from the low magnification image from each animal. Mature neuromuscular junctions (NMJs) were identified as BGX + cells co-localized with synaptophysin-puncta adjacent to phalloidin + muscle fibers. Mean percent mature NMJs was calculated by dividing the number of mature NMJs by the total number of BGX + receptors, averaged across replicates and by group.

For all statistical analyses following delayed nerve repair, since no differences were detected between the negative control groups (micro-column only and injury only/no transplantation), these samples were analyzed as a single group (acellular). Electrical conduction and evoked muscle response immediately after delayed repair (20 weeks following initial host axotomy) and at 1 month post delayed nerve repair (24 weeks following initial host axotomy) were performed by comparing the

mean CMAP amplitude, CNAP amplitude, and CNAP velocity using two-tailed unpaired Student's t-tests. Mean SMI35 expression and axon size, myelinated axon count, S100 β expression, AchR count, and percent mature NMJ were compared at 1 month post delayed nerve repair (24 weeks following initial host axotomy) using two-tailed unpaired Student's t-tests.

When differences existed between groups following one-way ANOVA, post-hoc Tukey's pair-wise comparisons were performed. For all statistical tests, $p < 0.05$ was required for significance and was performed in GraphPad Prism 9 (La Jolla California USA) for Windows 64 bit. Mean values presented as mean \pm standard deviation unless otherwise noted.

Data availability

Raw data is available upon request.

CRediT authorship contribution statement

Justin C. Burrell: Conceptualization, Methodology, Validation, Investigation, Data curation, Visualization, Writing – original draft, Writing – review & editing, Formal analysis, Project administration, Supervision. **Suradip Das:** Methodology, Writing – review & editing. **Franco A. Laimo:** Investigation. **Kritika S. Katiyar:** Investigation, Writing – review & editing. **Kevin D. Browne:** Methodology, Writing – review & editing. **Robert B. Shultz:** Investigation, Writing – review & editing. **Vishal J. Tien:** Methodology, Investigation. **Phuong T. Vu:** Methodology, Investigation. **Dmitriy Petrov:** Conceptualization, Methodology, Writing – review & editing. **Zarina S. Ali:** Conceptualization, Resources, Writing – review & editing. **Joseph M. Rosen:** Conceptualization, Writing – review & editing. **D. Kacy Cullen:** Conceptualization, Methodology, Writing – review & editing, Project administration, Resources, Supervision, Funding acquisition.

Declaration of competing interest

D.K.C is a co-founder of Axonova Medical, LLC, and Innervace, Inc. which are University of Pennsylvania spin-out companies focused on translation of advanced regenerative therapies to treat nervous system disorders. Multiple patents relate to the composition, methods, and use of tissue engineered nervous tissue [U.S. Patent 9,895,399 (D.K.C.), U.S. Patent 10,525,085 (D.K.C.), U.S. Patent Application 16/753,634 (D.K.C.), and U.S. Provisional Patent Application 62/937,489 (D.K.C. and J.C.B.)], microtissue-engineered neural networks [U.S. Patent Application 15/032,677 (D.K.C.), U.S. Patent Application 16/093,036 (D.K.C.), and U.S. Provisional Patent Application 63/209,639 (D.K.C., J.C.B., J.M.R.)], and innervated engineered tissue for organ modulation [U.S. Provisional Patent Application 62/758,203 (D.K.C. and S.D.)]. No other author has declared a potential conflict of interest.

Acknowledgements

The authors would like to thank Elizabeth Boyle for technical support. Financial support provided by the U.S. Department of Defense [CDMRP/JPC8-CRMRP W81XWH-16-1-0796 (Cullen) & CDMRP/PRORP W81XWH-19-1-0867 (Cullen & Das)], the Department of Veterans Affairs [BLR&D Merit Review I01-BX003748 (Cullen)], the National Institutes of Health [R44-NS108869 (Katiyar & Cullen), T32-EB005583 (Shultz), TL1-TR001880 (Burrell)], and the Center for Undergraduate Research and Fellowships at the University of Pennsylvania. Opinions, interpretations, conclusions and recommendations are those of the author(s) and are not necessarily endorsed by the Department of Defense, the Department of Veterans Affairs, or the National Institutes of Health.

Appendix A. Supplementary data

Supplementary data to this article can be found online at <https://doi.org/10.1016/j.bioactmat.2022.03.018>.

References

- [1] L.R. Robinson, Traumatic injury to peripheral nerves, *Muscle Nerve* 23 (2000) 863–873.
- [2] G.R. Evans, Peripheral nerve injury: a review and approach to tissue engineered constructs, *Anat. Rec.* 263 (2001) 396–404.
- [3] M. Siemionow, G. Brzezicki, Chapter 8: current techniques and concepts in peripheral nerve repair, *Int. Rev. Neurobiol.* 87 (2009) 141–172.
- [4] K. Brattain, Analysis of the Peripheral Nerve Repair Market in the United States, Magellan Medical Technology Consultants, Inc., 2012.
- [5] B. Battiston, et al., Chapter 11: tissue engineering of peripheral nerves, *Int. Rev. Neurobiol.* 87 (2009) 227–249.
- [6] C.J. Dy, J. Baty, M.J. Saeed, M.A. Olsen, D.A. Osei, A population-based analysis of time to surgery and travel distances for brachial plexus surgery, *J Hand Surg Am* 41 (2016) 903–909 e903.
- [7] A.M. Moore, Nerve transfers to restore upper extremity function: a paradigm shift, *Front. Neurol.* 5 (2014) 40.
- [8] B.J. Pfister, et al., Biomedical engineering strategies for peripheral nerve repair: surgical applications, state of the art, and future challenges, *Crit. Rev. Biomed. Eng.* 39 (2011) 81–124.
- [9] S.Y. Fu, T. Gordon, Contributing factors to poor functional recovery after delayed nerve repair: prolonged denervation, *J. Neurosci.* 15 (1995) 3886–3895.
- [10] D.C. Riley, et al., Polyethylene glycol-fused allografts produce rapid behavioral recovery after ablation of sciatic nerve segments, *J. Neurosci. Res.* 93 (2015) 572–583.
- [11] G.D. Bittner, M.L. Ballinger, M.A. Raymond, Reconnection of severed nerve axons with polyethylene glycol, *Brain Res* 367 (1986) 351–355.
- [12] G.D. Bittner, K.K. Rokkappanavar, J.D. Peduzzi, Application and implications of polyethylene glycol-fusion as a novel technology to repair injured spinal cords, *Neural Regen Res* 10 (2015) 1406–1408.
- [13] G.D. Bittner, D.R. Sengelaub, R.C. Trevino, C.L. Ghergherehchi, M. Mikesh, Robinson and madison have published no data on whether polyethylene glycol fusion repair prevents reinnervation accuracy in rat peripheral nerve, *J. Neurosci. Res.* 95 (2017) 863–866.
- [14] H.M. Fishman, G.D. Bittner, Vesicle-mediated restoration of a plasmalemmal barrier in severed axons, *News Physiol. Sci.* 18 (2003) 115–118.
- [15] C.L. Ghergherehchi, et al., Polyethylene glycol (PEG) and other bioactive solutions with neurorrhaphy for rapid and dramatic repair of peripheral nerve lesions by PEG-fusion, *J. Neurosci. Methods* 314 (2019) 1–12.
- [16] T.L. Krause, G.D. Bittner, Rapid morphological fusion of severed myelinated axons by polyethylene glycol, *Proc. Natl. Acad. Sci. U. S. A.* 87 (1990) 1471–1475.
- [17] T.L. Krause, R.E. Marquis, A.W. Lyckman, M.L. Ballinger, G.D. Bittner, Rapid artificial restoration of electrical continuity across a crush lesion of a giant axon, *Brain Res* 561 (1991) 350–353.
- [18] M. Mikesh, et al., Polyethylene glycol solutions rapidly restore and maintain axonal continuity, neuromuscular structures, and behaviors lost after sciatic nerve transections in female rats, *J. Neurosci. Res.* 96 (2018) 1223–1242.
- [19] K.W. Sexton, et al., Hydrophilic polymers enhance early functional outcomes after nerve autografting, *J. Surg.* 177 (2012) 392–400.
- [20] S. Yoo, M.P. Nguyen, M. Fukuda, G.D. Bittner, H.M. Fishman, Plasmalemmal sealing of transected mammalian neurites is a gradual process mediated by Ca(2+)-regulated proteins, *J. Neurosci. Res.* 74 (2003) 541–551.
- [21] S. Rotshenker, Wallerian degeneration: the innate-immune response to traumatic nerve injury, *J. Neuroinflammation* 8 (2011) 109.
- [22] L.A. Struzyna, J.P. Harris, K.S. Katiyar, H.I. Chen, D.K. Cullen, Restoring nervous system structure and function using tissue engineered living scaffolds, *Neural Regen Res* 10 (2015) 679–685.
- [23] C.C. Winter, et al., Transplantable living scaffolds comprised of micro-tissue engineered aligned astrocyte networks to facilitate central nervous system regeneration, *Acta Biomater* 38 (2016) 44–58.
- [24] L.A. Struzyna, et al., Anatomically inspired three-dimensional micro-tissue engineered neural networks for nervous system reconstruction, modulation, and modeling, *JoVE* 55609 (123) (2017) 1–14, <https://doi.org/10.3791/55609>.
- [25] K.S. Katiyar, et al., Three-dimensional tissue engineered aligned astrocyte networks to recapitulate developmental mechanisms and facilitate nervous system regeneration, *JoVE* 55848 (133) (2018) 1–17, <https://doi.org/10.3791/55848>.
- [26] J.C. O'Donnell, K.S. Katiyar, K.V. Panzer, D.K. Cullen, A tissue-engineered rostral migratory stream for directed neuronal replacement, *Neural Regen Res* 13 (2018) 1327–1331.
- [27] D.K. Cullen, et al., Microtissue engineered constructs with living axons for targeted nervous system reconstruction, *Tissue Eng.* 18 (2012) 2280–2289.
- [28] L.A. Struzyna, et al., Tissue engineered nigrostriatal pathway for treatment of Parkinson's disease, *J Tissue Eng Regen Med* 12 (2018) 1702–1716.
- [29] M.D. Serruya, et al., Engineered axonal tracts as “living electrodes” for synaptic-based modulation of neural circuitry, *Adv. Funct. Mater.* 28 (2018) 1701183.
- [30] P. Zadnik Sullivan, et al., Implantation of Engineered Axon Tracts to Bridge Spinal Cord Injury beyond the Glial Scar in Rats, *Tissue Eng Part A*, 2021.

- [31] K.S. Katiyar, L.A. Struzyna, S. Das, D.K. Cullen, Stretch growth of motor axons in custom mechanobioreactors to generate long-projecting axonal constructs, *J Tissue Eng Regen Med* 13 (2019) 2040–2054.
- [32] K.V. Panzer, et al., Tissue engineered bands of büngner for accelerated motor and sensory axonal outgrowth, *Front. Bioeng. Biotechnol.* 8 (2020).
- [33] Smith, D.H. et al. Tissue Engineered Grafts Exploit Axon-Facilitated Axon Regeneration and Pathway Protection to Facilitate Functional Recovery Following 5 Cm Peripheral Nerve Lesions in Swine. (Manuscript in Prep).
- [34] D. Petrov, et al., Neurorrhaphy in presence of polyethylene glycol enables immediate electrophysiological conduction in porcine model of facial nerve injury, *Front Surg* 9 (2022), 811544, <https://doi.org/10.3389/fsurg.2022.811544>.
- [35] S.Y. Fu, T. Gordon, Contributing factors to poor functional recovery after delayed nerve repair: prolonged axotomy, *J. Neurosci.* 15 (1995) 3876–3885.
- [36] T. Gordon, W. Tetzlaff, Regeneration-associated genes decline in chronically injured rat sciatic motoneurons, *Eur. J. Neurosci.* 42 (2015) 2783–2791.
- [37] S. Patodia, G. Raivich, Role of transcription factors in peripheral nerve regeneration, *Front. Mol. Neurosci.* 5 (2012) 8.
- [38] X. Fontana, et al., C-Jun in Schwann cells promotes axonal regeneration and motoneuron survival via paracrine signaling, *J. Cell Biol.* 198 (2012) 127–141.
- [39] P.J. Arthur-Farraj, et al., C-Jun reprograms Schwann cells of injured nerves to generate a repair cell essential for regeneration, *Neuron* 75 (2012) 633–647.
- [40] K.R. Jessen, R. Mirsky, The repair Schwann cell and its function in regenerating nerves, *J. Physiol.* 594 (2016) 3521–3531.
- [41] L.F. Domeshek, et al., Nerve transfers-A paradigm shift in the reconstructive ladder. *Plastic and reconstructive surgery, Global Open* 7 (2019).
- [42] J. Isaacs, et al., Effect of reverse end-to-side (supercharging) neurotization in long processed acellular nerve allograft in a rat model, *J Hand Surg Am* 44 (2019), 419 e411, 419 e410.
- [43] J. Isaacs, et al., Side-to-side supercharging nerve allograft enhances neurotrophic potential, *Muscle Nerve* 61 (2020) 243–252.
- [44] J.M. Hendry, M.C. Alvarez-Veronesi, A. Snyder-Warwick, T. Gordon, G. H. Borschel, Side-to-side nerve bridges support donor axon regeneration into chronically denervated nerves and are associated with characteristic changes in Schwann cell phenotype, *Neurosurgery* 77 (2015) 803–813.
- [45] X. Fang, et al., Reactivation of denervated Schwann cells by embryonic spinal cord neurons to promote axon regeneration and remyelination, *Stem Cell. Int.* 2019 (2019) 7378594.
- [46] C. Ruven, S.R. Badea, W.M. Wong, W. Wu, Combination treatment with exogenous GDNF and fetal spinal cord cells results in better motoneuron survival and functional recovery after avulsion injury with delayed root reimplantation, *J. Neuropathol. Exp. Neurol.* 77 (2018) 325–343.
- [47] W. Zhang, et al., Transplantation of embryonic spinal cord neurons to the injured distal nerve promotes axonal regeneration after delayed nerve repair, *Eur. J. Neurosci.* 45 (2017) 750–762.
- [48] R.M. Grumbles, P. Wood, M. Rudinsky, A.M. Gomez, C.K. Thomas, Muscle reinnervation with delayed or immediate transplant of embryonic ventral spinal cord cells into adult rat peripheral nerve, *Cell Transplant.* 11 (2017) 241–250.
- [49] K.S. Katiyar, et al., Tissue engineered axon tracts serve as living scaffolds to accelerate axonal regeneration and functional recovery following peripheral nerve injury in rats, *Front. Bioeng. Biotechnol.* 8 (2020) 492.
- [50] J.C. Burrell, et al., A porcine model of peripheral nerve injury enabling ultra-long regenerative distances: surgical approach, recovery kinetics, and clinical relevance, *Neurosurgery* 87 (2020) 833–846.
- [51] S. Das, et al., Innervation: the missing link for biofabricated tissues and organs, *NPJ Regen Med* 5 (2020) 11.
- [52] S. Das, et al., Pre-innervated tissue-engineered muscle promotes a pro-regenerative microenvironment following volumetric muscle loss, *Commun Biol* 3 (2020) 330.
- [53] J. Schindelin, et al., Fiji: an open-source platform for biological-image analysis, *Nat. Methods* 9 (2012) 676–682.